Research Article | Vol. 32, No. 21 / 7 Oct 2024 / *Optics Express* 36811

Optics EXPRESS

Pitfall in autocorrelation measurements of laser radiation

TORBEN FIEHLER,[1,*] CLARA SARACENO,[2] GÜNTER STEINMEYER,[3,4] AND ULRICH WITTROCK[1]

[1] *Photonics Laboratory, FH Münster, 48565 Steinfurt, Germany*
[2] *Photonics and Ultrafast Laser Science, Ruhr University Bochum, 44801 Bochum, Germany*
[3] *Max Born Institute for Nonlinear Optics and Short Pulse Spectroscopy, 12489 Berlin, Germany*
[4] *Department of Physics, Humboldt University, 12489 Berlin, Germany*
[*] *fiehler@fh-muenster.de*

Abstract: Spectrally broad laser radiation from continuous wave (cw) lasers can exhibit second-order autocorrelation traces virtually indistinguishable from those of mode-locked lasers. Consequently, based only on autocorrelations, one might erroneously conclude that a cw laser is mode-locked. This pitfall in interpretation can be avoided by carefully characterizing radio frequency transients and spectra. However, optoelectronics are often too slow for lasers with an axial mode spacing in the multi-GHz range. Carefully evaluated autocorrelations then remain the last resort for validating mode locking. We demonstrate in detail what needs to be observed. We compare autocorrelation measurements and calculations of a mode-locked titanium-sapphire (Ti:Sa) laser with 76 MHz repetition rate and a spectrally broad monolithic cw Ti:Sa laser and devise a new, additional measurement to safeguard against misinterpretation of their autocorrelations.

1. Introduction

Mode-locked lasers with pulse repetition rates in the GHz regime have attracted interest owing to their application in telecommunications [1], spectroscopy [2–8], in particular calibration of astronomical spectrographs [9–14], and quantum communication [15,16]. Confirming mode-locking of lasers with repetition rates of tens of GHz by resolving the pulse train in frequency or time requires very fast optoelectronic means. These are not available in some spectral regions. In such cases, optical autocorrelators are typically used. They can determine the duration of ultrashort pulses from a mode-locked laser, provided that the autocorrelator is sensitive enough as pulse energies at these repetition rates are typically in the pJ-range [17].

Many multi-GHz repetition rate lasers, such as mode-locked edge-emitting semiconductor lasers [18–20], vertical external cavity surface-emitting semiconductor lasers [21–23] and some mode-locked solid-state lasers [24–26] have standing-wave resonators where the gain medium extends to at least one of the resonator mirrors. If these lasers emit cw radiation, they can exhibit a spectral bandwidth of several nanometers due to strong spatial hole burning. Thus, the inverse of the spectral bandwidth lies within the subpicosecond range. Spatial hole burning is particularly pronounced in monolithic lasers with a standing-wave resonator because the gain medium extends across the entire resonator. When these spectrally broad lasers operate in cw mode, autocorrelators produce a coherence spike that can be easily misinterpreted as the autocorrelation of a short pulse. Therefore, characterizing a laser as mode-locked based only on autocorrelation measurements can be deceiving. Specifically, the second-order autocorrelation that is produced by spectrally broad longitudinal multimode cw radiation can resemble that of a mode-locked laser, as shown analytically in Section 2.3 and experimentally in Section 3.3. Both the first- and second-order autocorrelation exhibit a spike at zero time delay, indicating statistical fluctuations as they are present in cw laser radiation or thermal light [27–29]. This

#533567 https://doi.org/10.1364/OE.533567
Journal © 2024 Received 27 Jun 2024; revised 30 Aug 2024; accepted 5 Sep 2024; published 27 Sep 2024

Optics EXPRESS

spike is traditionally referred to as a "coherence spike" [30]. Its temporal width is proportional to the inverse of the spectral bandwidth and is often referred to as the coherence time of the laser because the first-order autocorrelation goes to zero on this time scale. However, the correlation between the longitudinal modes of a laser periodically reappears on the much longer time scale of integer multiples of the resonator round-trip time. This periodic correlation finally vanishes on an even longer timescale, given by the inverse linewidth of the modes. Note that the coherence spike appears in all autocorrelations, for example, that measured by a Fourier-transform infrared spectrometer (FTIR). The first-order autocorrelation is insensitive to the spectral phase and cannot be used to determine pulse durations.

One prominent example of a coherence spike was extensively discussed for a spectrally broad cw Nd:YLF laser exhibiting a spectral bandwidth of 0.6 nm, which would support pulses of a few picoseconds duration — if properly mode-locked [31]. Specifically, it was demonstrated that a bell-shaped autocorrelation alone does not suffice to confirm mode locking. The authors of Ref. [31] further emphasized the importance of a comprehensive characterization of mode-locked lasers, including autocorrelation, optical spectrum, and most importantly, an additional radio frequency (rf) spectrum as the minimum set of necessary experimental evidence. Improper mode locking would then show up as a more rapid roll-off of the intermode beats than supported by the bandwidth of the rf equipment under use. Although this method appears to be a rather surefire way to detect improper mode locking, its use becomes increasingly challenging for lasers operating at multi-GHz mode spacing, that is, only a very limited number of higher-order beat notes or even none can be detected by the rf analyzer, as the fastest commercially available photodetector in the wavelength range of 500 nm to 1200 nm has a 3 db bandwidth of 45 GHz [32]. Nevertheless, in this situation, autocorrelation measurements can still provide valuable insight, albeit limited, into whether a laser is properly mode-locked or not, which is the point we address in this paper.

Autocorrelations often exhibit a narrow cusp-like spike on top of a broad pedestal for the specific situation of a partially mode-locked laser when the laser emits irregular bursts of ultrashort pulses at a constant repetition rate [33]. The width of the broad pedestal of the autocorrelation then indicates the duration of the noise bursts. It determines the temporal resolution of pump-probe experiments. The width of the spike, however, is related to the average duration of the individual pulses within that burst. This spike is a coherence spike that is often referred to as a coherent artifact in more recent literature [34–36], cautioning against its misinterpretation as an autocorrelation of an ultrashort pulse. In the case of a spectrally broad cw laser, however, the pedestal-cusp structure does not appear in autocorrelations, as such a laser effectively emits an infinite noise burst. Consequently, the pedestal also shows an infinite temporal extent, and the autocorrelation exhibits an unsuspicious bell-shaped structure without shoulders, pedestals, or other indications of potential mode locking issues.

As an increasing number of multi-GHz repetition rate lasers have emerged in recent years, it is important to address the potential pitfall in characterizing these lasers with an autocorrelator, and discuss how to properly use an autocorrelator for confirming or disproving mode locking. To this end, we present, for the first time, comparative calculations and measurements of autocorrelations of mode-locked and cw lasers with broad spectral bandwidths. Specifically, we first discuss calculations of intensity and fringe-resolved autocorrelations for these lasers. We then compare these calculations with measured autocorrelations of a mode-locked titanium-sapphire (Ti:Sa) laser and those of a spectrally broad monolithic cw Ti:Sa laser. We show that similar autocorrelations are observed in both cases.

Optics EXPRESS

2. Second-order autocorrelations of laser light

2.1. Intensity autocorrelation (AC)

An intensity autocorrelation (AC), also called a background-free autocorrelation, is frequently used to determine the duration of ultrashort pulses and has the following expression [37]:

$$A_{\mathrm{AC}}(\tau) = \int_{-\infty}^{\infty} |E(t)E(t-\tau)|^2\, dt = \int_{-\infty}^{\infty} I(t)I(t-\tau)dt. \quad (1)$$

$E(t)$ is the electric field, and τ is the time delay. For simplicity, throughout this paper, we chose $I(t)$ to be defined as $I(t) = |E(t)|^2$, and $I(t)$ therefore represents a quantity that is proportional to the intensity but has units $\mathrm{V}^2/\mathrm{m}^2$. The AC is a symmetric function and the phase of $E(t)$ cannot be retrieved from it. Thus, the temporal shape of $E(t)$ cannot be determined either. If and only if the pulse shape is known or assumed, for example, as a sech^2 or Gaussian function, the AC provides information about the pulse duration because, in this case, the width of the intensity autocorrelation of the pulse is proportional to its temporal width.

A common setup used to produce an AC is a modified Michelson interferometer, in which the beam and its delayed copy are focused at different angles into a nonlinear crystal for second-harmonic generation (SHG). This setup is implemented in the autocorrelator pulseCheck 15 from APE Berlin GmbH, which is used in our experiments. It is schematically illustrated in Fig. 1(a).

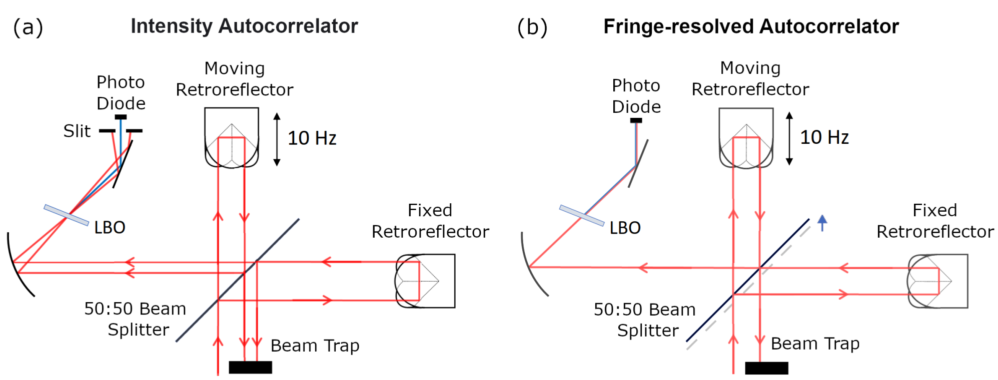

Fig. 1. The two setups of the pulseCheck 15 from APE Berlin GmbH. (a) Set up as an intensity autocorrelator. (b) Set up as a fringe-resolved autocorrelator. The blue arrow shows how the beam splitter has been shifted compared to the setup on the left.

2.2. Fringe-resolved autocorrelation (FRAC)

The pulseCheck 15 allows shifting the beam splitter towards the moving retroreflector so that the beams from both retroreflectors overlap at the beam splitter and propagate collinearly to the LBO crystal for SHG. In this case, a fringe-resolved autocorrelation (FRAC) is obtained, which is also called an interferometric autocorrelation. Figure 1(b) shows the setup of the fringe-resolved autocorrelator.

We need to recap the well-known mathematics of the FRAC in order to understand how the FRAC can be used to determine whether a laser is mode-locked. The FRAC is expressed as [38]

$$A_{\mathrm{FRAC}}(\tau) = \int_{-\infty}^{\infty} \left|[E(t) + E(t-\tau)]^2\right|^2 dt \quad (2)$$

This equation can be expanded to

$$A_{\mathrm{FRAC}}(\tau) = a_{\mathrm{bg}} + a_{\omega} + a_{2\omega} + a_{\mathrm{AC}} \quad (3)$$

with

$$a_{\mathrm{bg}} = 2\int_{-\infty}^{\infty} I(t)^2 dt \tag{4}$$

$$a_{\omega} = 4\int_{-\infty}^{\infty} [I(t) + I(t-\tau)]\,\mathrm{Re}[E(t)E^*(t-\tau)]dt \tag{5}$$

$$a_{2\omega} = 2\int_{-\infty}^{\infty} \mathrm{Re}[E^2(t)E^{*2}(t-\tau)]dt \tag{6}$$

$$a_{\mathrm{AC}} = 4\int_{-\infty}^{\infty} I(t)I(t-\tau)dt = 4A_{\mathrm{AC}}(\tau) \tag{7}$$

Equation (3) shows that the FRAC consists of four parts. The first part (a_{bg}) is the background intensity. The second part (a_{ω}) is the real part of the field autocorrelation of the fundamental beam if the term $[I(t) + I(t-\tau)]$ is omitted. This is reasonable because for different delays τ, $[I(t) + I(t-\tau)]$ can only have values between $I(t)$ and $2I(t)$, whereas the product of the fields in $\mathrm{Re}[E(t)E^*(t-\tau)]$ changes between $-E(t)^2$ and $E(t)^2$ and is much more sensitive to the temporal profile of the electric field. As a result, the change in amplitude for $[I(t) + I(t-\tau)]$ is smaller than that for $\mathrm{Re}[E(t)E^*(t-\tau)]$ and therefore has a lower impact on the product of the two terms. The third part ($a_{2\omega}$) is the real part of the field autocorrelation of the second harmonic. The last part (a_{AC}) is equal to four times the intensity autocorrelation. The four parts of the FRAC given by Eqs. (4)–(7), calculated for a transform-limited 200 fs pulse, are shown in Fig. 2. The interference fringes in Fig. 2(b) and 2(c) appear as blue-filled areas because the fringes have a period equal to the inverse of the light frequency and are not resolved in the plot.

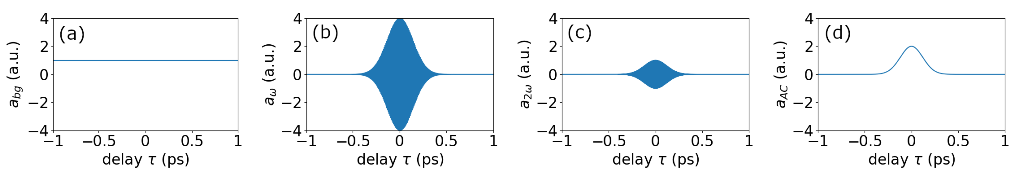

Fig. 2. Calculated contributions to the FRAC according to Eq. (4)–(7) for a transform-limited 200 fs pulse. (a) Background intensity (a_{bg}), (b) modified real part of the field autocorrelation of the fundamental beam (a_{ω}), (c) real part of the field autocorrelation of the second harmonic ($a_{2\omega}$) and (d) intensity autocorrelation (a_{AC}). When summed, all four parts yield the FRAC trace shown in blue in Fig. 3(a) and Fig. 4(g). Note that the fringe period in (b) is determined by the fundamental frequency according to Eq. (5) whereas the fringe period in (c) is determined by the second harmonic frequency according to Eq. (6)

Similar to the AC, the FRAC cannot provide the temporal phase of the electrical field either. However, the FRAC can reveal whether a laser is mode-locked or not. The FRAC of a chirped pulse has wings with a lower contrast of the high-frequency interference fringes compared to an unchirped pulse [37]. This can be seen by comparing the calculated FRAC of a transform-limited 200 fs pulse in Fig. 3(a) and a chirped 800 fs pulse in Fig. 3(b). Introducing extra-cavity dispersion to a laser that produces mode-locked pulses changes its chirp and, consequently, the interference contrast of the wings of the FRAC. Introducing the same extra-cavity dispersion to a spectrally broad cw laser does not change the FRAC. This is because there is no phase coherence between the axial modes of a cw laser. Therefore, changing the spectral phases of these modes by introducing dispersion cannot have any consequences. The FRAC of a cw laser simply shows the coherence spike.

The mathematical reason for the reduced interference contrast in the wings of the FRAC of chirped pulses is that only a_{AC} in Eq. (7) broadens when the spectral phase of the electric field is altered. a_{ω} in Eq. (5) and $a_{2\omega}$ in Eq. (6) are both field autocorrelations whose width

Optics EXPRESS

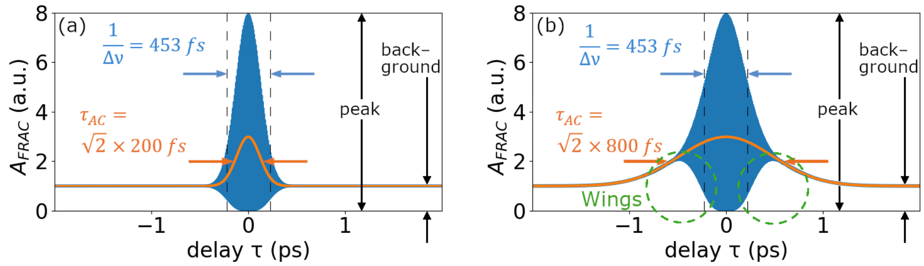

Fig. 3. (a) The blue curve is the calculated FRAC of a transform-limited 200 fs Gaussian-shaped pulse. The orange curve is the calculated low-pass filtered FRAC, which is the sum of a_{bg} and a_{AC} from Eq. (4) and (7). Its width is the pulse duration multiplied by the deconvolution factor for a Gaussian-shaped pulse. Dashed black lines indicate the inverse spectral bandwidth $1/\Delta\nu$. (b) Calculated FRAC of the same pulse as in (a) but broadened to 800 fs due to group delay dispersion. The FRAC of the chirped pulse in (b) shows wings at ± 0.5 ps, where the contrast of the interference fringes is reduced. These wings are marked by dashed green circles.

is proportional to the inverse of the bandwidth. A field autocorrelation is not sensitive to the spectral phase of the electric field and therefore does not broaden for chirped pulses. This is also why a second-order autocorrelation using a nonlinear crystal is required. A simple Michelson interferometer without such a nonlinear crystal produces a first-order field autocorrelation that only shows a coherence spike.

2.3. Autocorrelations of ultrashort pulses and cw radiation

We now compare the simulated AC and FRAC of a transform-limited ultrashort Gaussian pulse from a mode-locked laser with the simulated AC and FRAC of radiation from a spectrally broad cw laser. Both lasers have a spectral bandwidth of 3.4 nm. The results are shown in Fig. 4.

We use blue traces in our graphs for mode-locked radiation and red traces for cw radiation throughout this paper. The filled region in all FRAC traces shown in this paper represents unresolved high-frequency interference fringes. Figure 4(a)–(d) show the intensity, power spectral density, and spectral phase of the two lasers. The AC in Fig. 4(e) shows a background-free autocorrelation for the mode-locked laser. Figure 4(f) shows this curve for the cw laser. The shape of this curve resembles that shown in Fig. 4(e), yet with a strong background that is half of the maximum. At zero delay, the electric fields from both correlator arms add up linearly, which quadruples the SHG intensity compared to the single beam. If the two beams are delayed by more than their coherence time then the square root of their fields add up, which only doubles the SHG intensity and gives rise to the background in Figure 4(f). Ignoring this additional background has misled observers in the past to conclude that cw lasers produce ultrashort pulses if the strong background of the curve in Fig. 4(f) is overlooked or disregarded as a noise floor. Not recognizing this background is the pitfall we mentioned in the introduction of this paper. Indeed, this strong background of the autocorrelation in Fig. 4(f) is the only indication that the modes of the laser are not locked in phase. Assuming a complete lack of coherence between the longitudinal laser modes, a peak-to-background ratio of only $2/1 = 2$ results [39]. This is also confirmed in our simulations, cf. Fig. 4(f). Larger but finite peak-background ratios may arise in case of partial coherence [33,39].

The FRAC of cw radiation in Fig. 4(h) resembles the FRAC trace of the mode-locked laser in Fig. 4(g), but has a stronger background intensity. Again, this higher background is the only indication that the laser is not mode-locked. The peak-to-background ratio of the FRAC of mode-locked radiation is $8/1 = 8$ compared to $8/2 = 4$ for cw radiation.

Optics EXPRESS

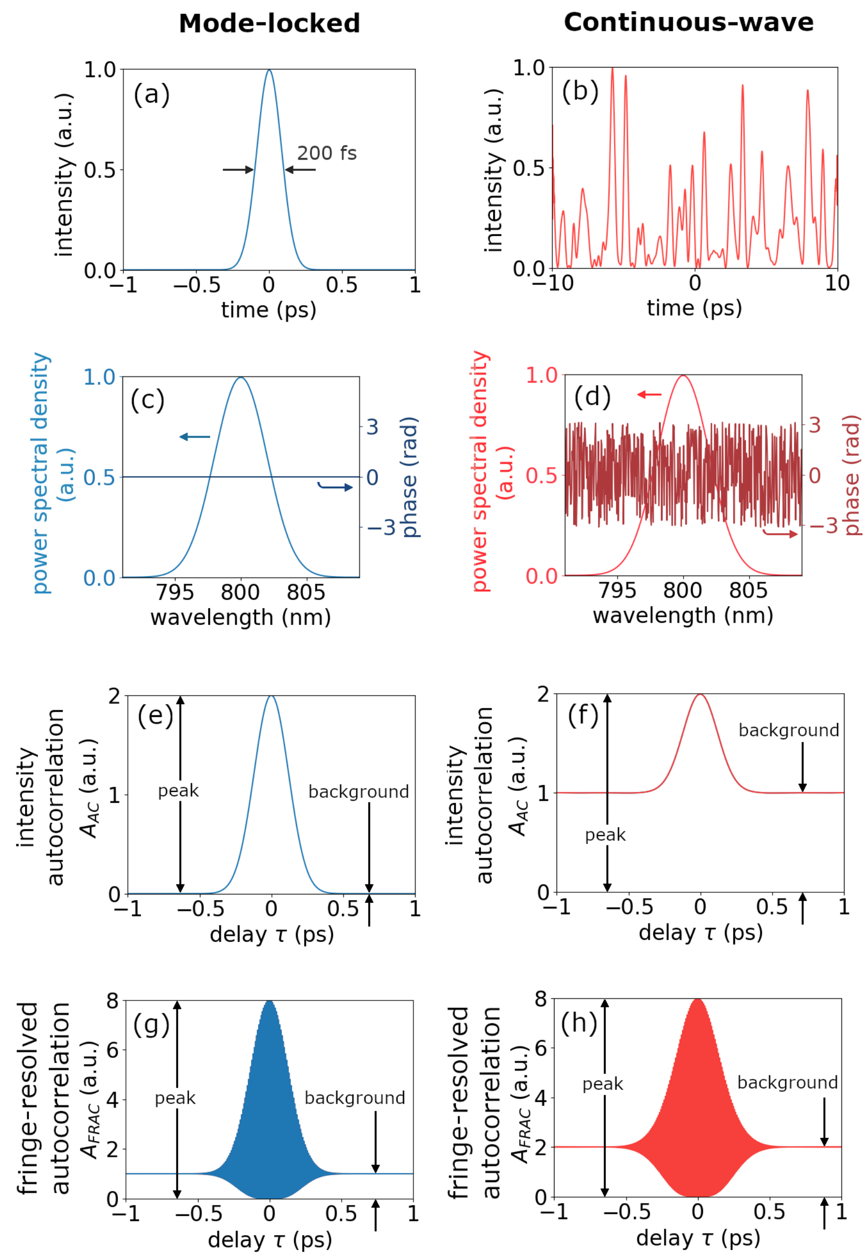

Fig. 4. Simulated autocorrelations of a mode-locked laser (left column, blue) and a cw laser (right column, red), both with 3.4 nm wide Gaussian power spectral densities. (a), (b) Intensity in the time-domain; (c), (d) power spectral density and phase; (e), (f) intensity autocorrelation; (g), (h) fringe-resolved autocorrelation.

Similar to Fig. 2, Fig. 5 shows the four contributions to the FRAC trace from Eq. (4)–(7) calculated for both the mode-locked laser and cw radiation, the sum of which yields the FRAC traces in Fig. 4(g) and 4(h), respectively. From Fig. 5(d), it can be seen that the higher background intensity in the FRAC trace for cw radiation is caused by the part that is due to the intensity autocorrelation a_{AC} in Eq. (7). As shown in Fig. 5(a) and 5(c), there is no difference between

Optics EXPRESS

the mode-locked laser and cw radiation for a_{bg} and $a_{2\omega}$. Only the trace for a_ω in Fig. 5(b) is slightly broader for cw radiation than for the mode-locked laser. This is caused by the factor $[I(t) + I(t-\tau)]$ in Eq. (5). As previously discussed, the temporal shape and temporal width of the field autocorrelations a_ω and $a_{2\omega}$ are independent of the phase relationship between the spectral components of the laser. It is only a_{AC} that contains information about the phase relationship, making it the only indicator of whether a laser is in cw operation or mode-locked.

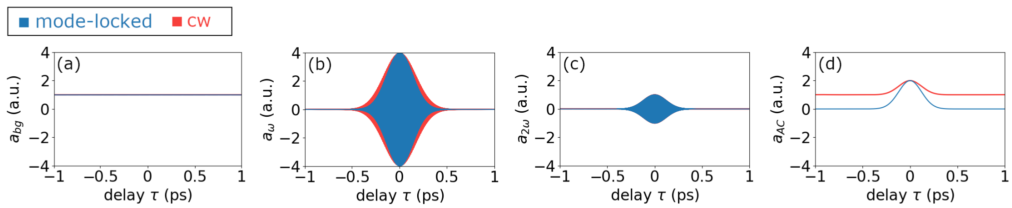

Fig. 5. Calculated contributions to the FRAC according to Eq. (4)–(7) for mode-locked radiation in blue and for cw laser radiation in red. (a) Background intensity (a_{bg}), (b) modified real part of the field autocorrelation of the fundamental beam (a_ω), (c) real part of the field autocorrelation of the second harmonic ($a_{2\omega}$) and (d) intensity autocorrelation (a_{AC}). (a) and (c) are identical for both lasers. Both lasers have a power spectral density and phase as shown in Fig. 4(c) and 4(d). All four parts sum up to the FRAC traces shown in Fig. 4(g) and 4(h). As already mentioned in the caption of Fig. 2, the periods of the unresolved interference fringes of (b) and (c) are different.

3. Experiments

3.1. Introduction

In this section, we compare measured autocorrelations of a commercial mode-locked Ti:Sa laser and a home-built cw Ti:Sa laser. Both lasers have nearly identical center wavelengths of about 785 nm and similar spectral bandwidths of about 8 nm, as shown in Fig. 6. The mode-locked laser is a Mira Optima 900-D from Coherent, which is a tunable femtosecond Ti:Sa laser system with 76 MHz repetition rate.

3.2. Autocorrelation measurements of the mode-locked Mira Optima 900-D

Figure 7 shows the AC and FRAC of the mode-locked Mira laser. The background is barely visible as the AC has a peak-to-background ratio of 1/0.04 = 25. As shown in Fig. 4(f), this ratio does not exceed 2 for cw radiation. Therefore, we can conclude that the laser is mode-locked. For the FRAC, the peak-to-background ratio is 7.3. This ratio also confirms mode locking because the peak-to-background ratio of the FRAC does not exceed 4 for cw radiation, as shown in Fig. 4(h). The deviation from the ideal ratio of 8 can be attributed to alignment errors.

We also measured autocorrelations of the Mira laser in cw operation to see if we could detect a coherence spike similar to that simulated in Fig. 4(f) and 4(h). Mode locking was suppressed by opening the slit that is used for hard-aperture Kerr-lens mode locking. Figure 8 shows the power spectral density, the AC, and the FRAC during cw operation. Both autocorrelations show only the peak of the coherence spike because the spectral bandwidth drops to below 10 GHz. The inverse of this spectral bandwidth is more than 100 ps. This is longer than the maximum scan range of our autocorrelator which is 15 ps. A coherence spike, as seen in the simulated AC and FRAC in Fig. 4(f) and 4(h), can only be observed for cw lasers that have such a large spectral bandwidth that its inverse is smaller than the scan range of the autocorrelator. This illustrates that the problem of misleading autocorrelation traces showcased in our paper becomes increasingly important for lasers that are designed to produce ultrashort pulses with very high repetition rates.

Optics EXPRESS

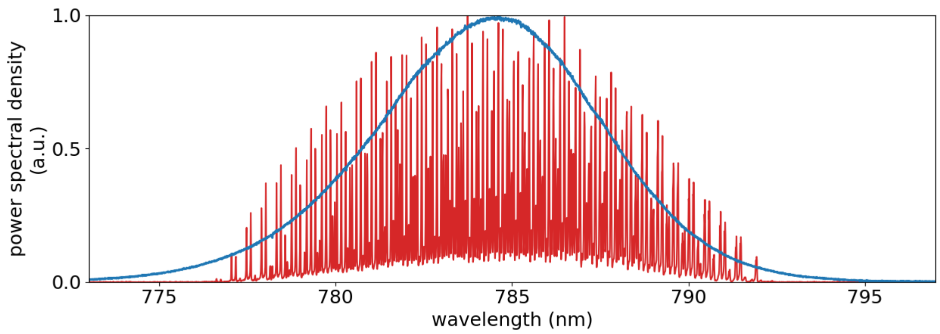

Fig. 6. Power spectral density of the mode-locked Mira laser (blue) and our cw Ti:Sa laser (red), both measured with a spectrometer (Horiba HR-640) with 20 pm spectral resolution. The spectral bandwidth is about 9 nm for our cw Ti:Sa laser and 7.3 nm for the Mira laser. The axial modes of our cw Ti:Sa laser are resolved by the spectrometer due to their large mode spacing of 28 GHz while the modes of the Mira laser with 76 MHz mode spacing are not resolved.

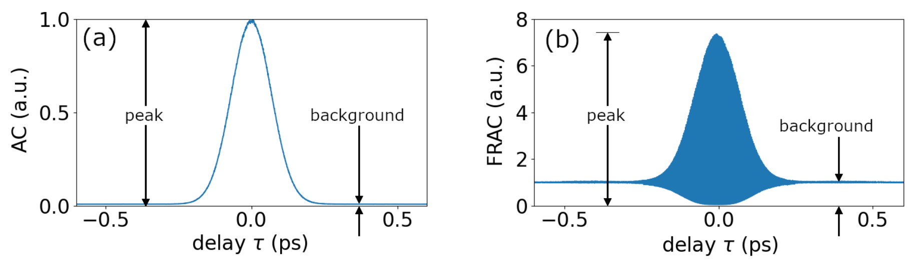

Fig. 7. (a) AC of the mode-locked Mira laser. The pulse duration is 116 fs, assuming a Gaussian-shaped pulse. Assuming a Gaussian-shaped pulse results in a better fit to the measured AC trace than assuming a sech^2-shaped pulse. The peak-to-background ratio is 25, and the time-bandwidth product is 0.41. (b) FRAC of the mode-locked Mira laser, showing a peak-to-background ratio of 7.3 and no sign of chirp.

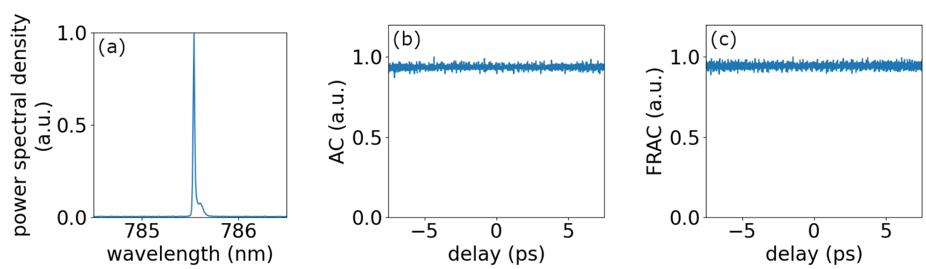

Fig. 8. (a) Power spectral density, (b) intensity autocorrelation and (c) fringe-resolved autocorrelation of the Mira laser while in cw operation. Given the limited scan range of the autocorrelator and the narrow bandwidth of the Mira laser in cw operation, we can only observe a delay-independent AC and FRAC signals. These flat traces are nothing but fractions of the central plateau of a very wide coherence spike. We estimate that a scan range of several nanoseconds would be required to resolve the coherence spike.

We then mode-locked the Mira laser again and intentionally misaligned the autocorrelator and laser with respect to each other, such that the beam entered the autocorrelator at an angle of a few milliradians, which reduces the peak-to-background ratio of the autocorrelation trace. Further

Optics EXPRESS

misalignments also included insufficient collimation of the beam and, while measuring the FRAC, reducing the collinearity of the two pulse copies. With these misalignments, we attempted to produce AC and FRAC traces similar to those of a spectrally broad cw laser to further illustrate the ambiguity of autocorrelation measurements once the peak-to-background ratio is less than 2 for AC traces or 4 for FRAC traces. The AC in Fig. 9(a) has a peak-to-background of $1/0.55 = 1.8$ compared to 25 in Fig. 7(a). For the FRAC, we reduced the peak-to-background ratio to 3.8 in Fig. 9(b) compared to 7.3 in Fig. 7(b). Note that the FRAC was more sensitive to misalignments than the AC.

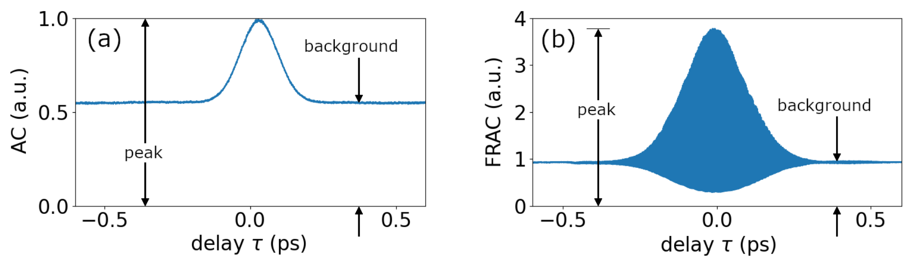

Fig. 9. Autocorrelations of the mode-locked Mira laser while the autocorrelator was deliberately misaligned as described in the text. (a) Intensity autocorrelation with a peak-to-background ratio of 1.8 instead of 25 in Fig. 7(a). (b) Fringe-resolved autocorrelation showing a peak-to-background ratio of 3.8 instead of 7.3 in Fig. 7(b).

Our experiment shows that the peak-to-background ratios obtained from mode-locked lasers can be even lower than those obtained from cw lasers with a well-aligned autocorrelator, which are 2 and 4 for the AC and FRAC, respectively (see Fig. 4(f) and 4(h)), compared to 1.8 and 3.8 in Fig. 9. In this case, no conclusion can be drawn regarding whether the laser is mode-locked.

3.3. Autocorrelation measurements of a monolithic cw Ti:Sa laser

In this section, we present experimental evidence of the aforementioned pitfall in autocorrelation measurements. To this end, we use a home-built monolithic Ti:Sa laser consisting of a disk-shaped Ti:Sa crystal where both planar optical surfaces carry dispersive resonator mirror coatings. The laser resonator becomes stable due to thermal lensing generated by the absorbed pump light. The Ti:Sa disk is 3 mm thick, which results in an axial mode spacing of 28 GHz. This laser was designed for Kerr-lens mode locking at a repetition rate of 28 GHz, but mode locking could not be achieved with this particular crystal. The laser design is illustrated in Fig. 10. Our similar-designed monolithic laser with a 5 mm thick Ti:Sa disk recently showed mode locking at a repetition rate of 17 GHz [40]. Further details of this mode-locked laser will be presented in a separate publication.

The spectrum of the 3 mm thick monolithic cw Ti:Sa laser is approximately 9 nm broad, as shown in Fig. 6. Therefore, the inverse of the spectral bandwidth is about 230 fs. One reason for the broad spectrum is strong spatial hole burning in the inversion by the axial modes. As in a microchip laser, the population inversion in our laser extends to the ends of the resonator because the resonator mirror coatings are attached to the gain medium. Therefore, a significant fraction of the inversion can be accessed only by axial modes with large wavelength differences from the central wavelength. This is also known as the gain-at-the-end effect [41]. Other sources of spectral broadening are possibly four-wave mixing [42] and modulation instabilities [43].

1 W of the output power of our cw Ti:Sa laser was coupled into the autocorrelator. The autocorrelations are shown in Fig. 11. The AC has a peak-to-background ratio of $1/0.55 = 1.8$ and the FRAC trace has a ratio of 3.7. The shapes of both autocorrelation traces in Fig. 11 are similar to those of the simulated AC and FRAC traces in Fig. 4(f) and 4(h). The deviation from

Optics EXPRESS

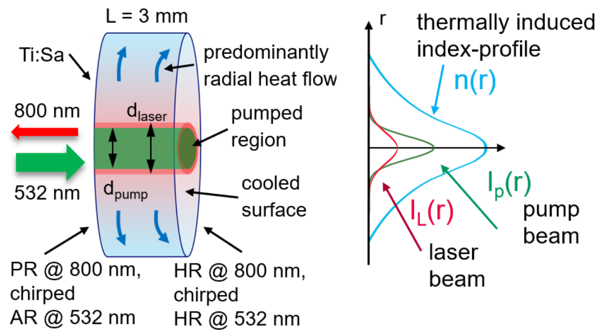

Fig. 10. Schematic of our monolithic cw Ti:Sa laser. The Ti:Sa crystal with its coatings creates the shown monolithic plane-plane resonator. The heat deposited by the pump laser creates the shown thermally induced index-profile that we have calculated with a finite element analysis using COMSOL. With a suitable pump spot diameter, both the pump beam and the laser beam become eigenmodes of the thermally-induced gradient index medium.

the ideal ratios of 2 for the AC and 4 for the FRAC is most likely due to alignment errors. The full-width-at-half-maximum of the coherence spike is 193 fs. Note that the autocorrelations shown in Fig. 11 are also similar to those of the mode-locked Mira laser measured with a misaligned autocorrelator, as shown in Fig. 9. Thus, a strong background in autocorrelation traces alone is not sufficient to prove that a laser is not mode-locked.

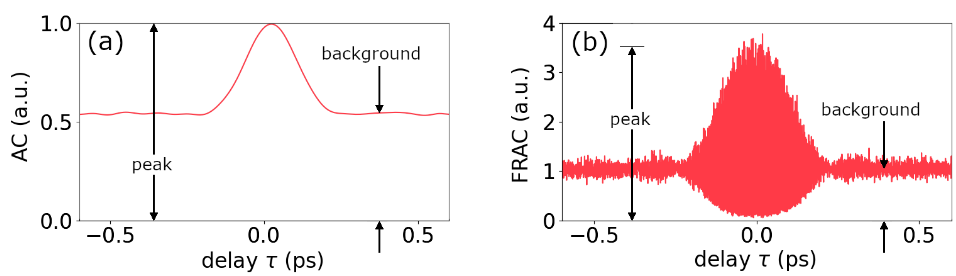

Fig. 11. (a) Intensity autocorrelation of the spectrally broad cw radiation from our monolithic cw Ti:Sa laser with a peak-to-background ratio of 1.8. (b) Fringe-resolved autocorrelation of the same laser, showing a peak-to-background ratio of 3.7.

We found that a reliable method for confirming at least partial mode locking is to introduce group delay dispersion (GDD) and observe the change in the width of the autocorrelation. For ultrashort pulses, introducing GDD leads to pulse broadening or pulse compression, both of which changes the autocorrelation width. Introducing GDD to cw radiation does not change the width of the autocorrelation because there is no coherent relationship between the phases of the axial modes of the laser. We introduced up to 10^6 fs^2 negative GDD with a Treacy grating arrangement described in [44] to our monolithic Ti:Sa laser and observed no change in the width of the autocorrelation. Therefore, the laser is not mode-locked.

The autocorrelator pulseCheck 15 from APE Berlin requires an average power of at least 100 mW in order to produce an autocorrelation of our cw Ti:Sa laser. At this power, the signal was weak, and even at an average power of 1 W, it remained noisy. This can be seen in Fig. 11. Both, the power requirement of autocorrelators and the need for a sufficiently broad spectrum in cw operation may explain why the pitfall we describe has not received much attention in the past; we found only two publications that mentioned the possibility of misinterpreting the coherence spike of a cw laser as proof of mode locking. Wilcox *et al.* [31] showed that a coherence spike is

Optics EXPRESS

present in the autocorrelation of a spectrally broad cw Nd:YLF laser to demonstrate that such a spike should not be taken as evidence of mode locking. Escoto *et al.* [45] only mentioned this in passing. Semiconductor lasers with a mode spacing in the multi-GHz range are spectrally broad, but typically achieve maximum average powers of only 100 mW to 200 mW [9,18,22]. If these lasers do not mode-lock, the coherence spike may remain unnoticed or disappear in the noise floor.

4. Conclusion

We have shown that the second-order autocorrelation can be a powerful tool for confirming mode locking of lasers with a multi-GHz repetition rate. However, a severe potential pitfall is lurking unless utmost care is taken in analyzing the autocorrelation trace.

From an engineering point of view, a monolithic architecture is ideal for mode-locked lasers with repetition rates of more than 10 GHz, as the round-trip optical path length of the resonator becomes less than 1.5 cm. Such short resonators lead to strong spatial hole burning which is further enhanced in monolithic architectures where the gain medium is in contact with the resonator mirrors. Spatial hole burning as well as four-wave mixing cause spectral broadening, which results in broadband longitudinal cw multimode operation when these lasers are not mode-locked. In this case, the autocorrelation can show an isolated pedestal-free coherence spike that can easily be mistaken as a proof of mode locking. However, careful inspection of the autocorrelation trace according to the following checklist can reveal whether a laser is mode-locked:

- The laser is mode-locked if the peak-to-background ratio is greater than 2 for the AC and greater than 4 for the FRAC.
- If the peak-to-background ratio is smaller than 2 for the AC or smaller than 4 for the FRAC, no definite conclusion can be drawn because these values can appear just as well for a spectrally broad cw laser and for a mode-locked laser due to misalignment of the autocorrelator or strong noise.
- The laser is at least partially mode-locked if the width of the autocorrelation changes after introducing dispersion to the beam. For a cw laser, dispersion neither changes the width of the AC nor that of the FRAC.
- A FRAC that has wings with reduced contrast of the interference can additionally confirm mode locking as they can only be observed for chirped mode-locked pulses and not for cw radiation.
- A narrow cusp-like spike on top of a broad pedestal indicates that the laser is only partially mode-locked.

As optoelectronic means offer no alternative at repetition rates above tens of GHz, careful analysis of autocorrelation measurements then remains the last resort for confirming mode locking of lasers with such repetition rates.

Funding. Deutsche Forschungsgemeinschaft (WI 1939/6-1).

Acknowledgments. We would like to thank Martin Saraceno (Photonics and Ultrafast Laser Science, Ruhr University Bochum), Martin Hofmann (Photonics and Terahertz Technology, Ruhr University Bochum), and Mateusz Ibek (APE Berlin GmbH) for their helpful advice and discussions.

Disclosures. The authors declare no conflicts of interest.

Data availability. Data underlying the results presented in this paper are not publicly available at this time but may be obtained from the authors upon reasonable request.

Optics EXPRESS

Supplemental document. See Supplement 1 for supporting content.

References

1. H. Hu and L. K. Oxenløwe, "Chip-based optical frequency combs for high-capacity optical communications," Nanophotonics **10**(5), 1367–1385 (2021).
2. B. Willenberg, C. R. Phillips, J. Pupeikis, *et al.*, "THz time-domain spectroscopy with a GHz single-cavity dual-comb laser," in *Conference on Lasers and Electro-Optics Europe European Quantum Electronics Conference* (2023).
3. T. Voumard, J. Darvill, T. Wildi, *et al.*, "1-GHz dual-comb spectrometer with high mutual coherence for fast and broadband measurements," Opt. Lett. **47**(6), 1379–1382 (2022).
4. M. Maiuri, M. Garavelli, and G. Cerullo, "Ultrafast spectroscopy: State of the art and open challenges," J. Am. Chem. Soc. **142**(1), 3–15 (2020).
5. I. Coddington, N. Newbury, and W. Swann, "Dual-comb spectroscopy," Optica **3**(4), 414–426 (2016).
6. K. Twayana, I. Rebolledo-Salgado, E. Deriushkina, *et al.*, "Spectral interferometry with frequency combs," Micromachines **13**(4), 614 (2022).
7. O. Kliebisch, D. C. Heinecke, and T. Dekorsy, "Ultrafast time-domain spectroscopy system using 10 GHz asynchronous optical sampling with 100 kHz scan rate," Opt. Express **24**(26), 29930–29940 (2016).
8. K. J. Mohler, B. J. Bohn, M. Yan, *et al.*, "Dual-comb coherent Raman spectroscopy with lasers of 1-GHz pulse repetition frequency," Opt. Lett. **42**(2), 318–321 (2017).
9. Y. S. Cheng, D. Xiao, R. A. McCracken, *et al.*, "Laser-frequency-comb calibration for the Extremely Large Telescope: an OPO-based infrared astrocomb covering the H and J bands," J. Opt. Soc. Am. B **38**(7), A15–A20 (2021).
10. T. Herr and R. A. McCracken, "Astrocombs: Recent advances," IEEE Photon. Technol. Lett. **31**(23), 1890–1893 (2019).
11. R. A. McCracken, É. Depagne, R. B. Kuhn, *et al.*, "Wavelength calibration of a high resolution spectrograph with a partially stabilized 15-GHz astrocomb from 550 to 890 nm," Opt. Express **25**(6), 6450–6460 (2017).
12. K. Nakamura, K. Kashiwagi, S. Okubo, *et al.*, "Erbium-doped-fiber-based broad visible range frequency comb with a 30 GHz mode spacing for astronomical applications," Opt. Express **31**(12), 20274–20285 (2023).
13. Y. S. Cheng, K. Dadi, T. Mitchell, *et al.*, "Continuous ultraviolet to blue-green astrocomb," Nat. Commun. **15**(1), 1466 (2024).
14. E. Chae, E. Kambe, K. Motohara, *et al.*, "Compact green Ti:sapphire astro-comb with a 43 GHz repetition frequency," J. Opt. Soc. Am. B **38**(7), A1 (2021).
15. M. Hussain, D. Heinrich, M. Guevara-Bertsch, *et al.*, "Ultraviolet laser pulses with multigigahertz repetition rate and multiwatt average power for fast trapped-ion entanglement operations," Phys. Rev. Appl. **15**(2), 024054 (2021).
16. R.-B. Jin, R. Shimizu, I. Morohashi, *et al.*, "Efficient generation of twin photons at telecom wavelengths with 2.5 GHz repetition-rate-tunable comb laser," Sci. Rep. **4**(1), 7468 (2014).
17. D. N. Fittinghoff, J. L. Bowie, J. N. Sweetser, *et al.*, "Measurement of the intensity and phase of ultraweak, ultrashort laser pulses," Opt. Lett. **21**(12), 884–886 (1996).
18. N. Kleemann, N. Surkamp, P. Scherer, *et al.*, "Investigation of passive mode-locking and self-mode-locking in two-section monolithic QD and QW lasers," in *Novel In-Plane Semiconductor Lasers XXIII*, vol. 12905 (SPIE, 2024), p. 129050R.
19. J. H. Marsh and L. Hou, "Mode-locked laser diodes and their monolithic integration," IEEE J. Sel. Top. Quantum Electron. **23**(6), 1–11 (2017).
20. K. Merghem, A. Akrout, A. Martinez, *et al.*, "Pulse generation at 346 GHz using a passively mode locked quantum-dash-based laser at 1.55 um," Appl. Phys. Lett. **94**(2), 021107 (2009).
21. J. Nürnberg, C. G. E. Alfieri, D. Waldburger, *et al.*, "A single free-running dual-comb MIXSEL for fast and precise distance measurements," in *Conference on Lasers and Electro-Optics Europe European Quantum Electronics Conference* (Optica Publishing Group, 2019).
22. M. Mangold, C. A. Zaugg, S. M. Link, *et al.*, "Pulse repetition rate scaling from 5 to 100 GHz with a high-power semiconductor disk laser," Opt. Express **22**(5), 6099–6107 (2014).
23. T. Malica, K. Panajotov, E. A. Avrutin, *et al.*, "Passively mode-locked high-frequency dual-VCSEL system," Opt. Express **31**(5), 8296–8306 (2023).
24. H. Ostapenko, T. Mitchell, P. Castro-Marin, *et al.*, "Three-element, self-starting Kerr-lens-modelocked 1-GHz Ti:sapphire oscillator pumped by a single laser diode," Opt. Express **30**(22), 39624–39630 (2022).
25. M. T. Chang, H. C. Liang, K. W. Su, *et al.*, "Dual-comb self-mode-locked monolithic Yb:KGW laser with orthogonal polarizations," Opt. Express **23**(8), 10111–10116 (2015).
26. T. D. Shoji, W. Xie, K. L. Silverman, *et al.*, "Ultra-low-noise monolithic mode-locked solid-state laser," Optica **3**(9), 995–998 (2016).
27. J. R. Klauder, M. A. Duguay, J. A. Giordmaine, *et al.*, "Correlation effects in the display of picosecond pulses by two-photon techniques," Appl. Phys. Lett. **13**(5), 174–176 (1968).
28. L. Mandel and E. Wolf, "Coherence properties of optical fields," Rev. Mod. Phys. **37**(2), 231–287 (1965).
29. R. Loudon, *The Quantum Theory of Light* (Oxford University, 2000), 3rd ed.
30. J.-C. M. Diels, J. J. Fontaine, I. C. McMichael, *et al.*, "Control and measurement of ultrashort pulse shapes (in amplitude and phase) with femtosecond accuracy," Appl. Opt. **24**(9), 1270–1282 (1985).

Optics EXPRESS

31. K. G. Wilcox and A. C. Tropper, "Comment on sesam-free mode-locked semiconductor disk laser," Laser Photonics Reviews **7**(3), 422–423 (2013).
32. Newport Spectra-Physics GmbH, High Speed Detector and Receiver User Manual (2023), Rev. A.
33. M. Rhodes, G. Steinmeyer, J. Ratner, *et al.*, "Pulse-shape instabilities and their measurement," Laser Photonics Reviews **7**(4), 557–565 (2013).
34. R. Trebino, "The most important paper you've never read," Opt. Photon. News **31**(1), 46–53 (2020).
35. J. Ratner, G. Steinmeyer, T. C. Wong, *et al.*, "Coherent artifact in modern pulse measurements," Opt. Lett. **37**(14), 2874–2876 (2012).
36. R. Trebino, R. Jafari, S. A. Akturk, *et al.*, "Highly reliable measurement of ultrashort laser pulses," J. Appl. Phys. **128**(17), 171103 (2020).
37. B. E. A. Saleh, M. C. Teich, and J. W. Goodman, *Fundamentals of Photonics* (John Wiley Sons, Ltd., 1991).
38. J.-C. Diels and W. Rudolph, *Ultrashort Laser Pulse Phenomena* (Elsevier, 2006), 2nd ed.
39. H. P. Weber and H. G. Danielmeyer, "Multimode effects in intensity correlation measurements," Phys. Rev. A **2**(5), 2074–2079 (1970).
40. T. Fiehler and U. Wittrock, "17 GHz monolithic self-starting Kerr-lens mode-locked Titanium-Sapphire laser," in *DPG Spring Meeting Greifswald* (2023), Talk K2.3.
41. B. Braun, K. J. Weingarten, F. X. Kärtner, *et al.*, "Continuous-wave mode-locked solid-state lasers with enhanced spatial hole burning," Appl. Phys. B **61**(5), 429–437 (1995).
42. G. P. Agrawal, *Nonlinear Fiber Optics* (Elsevier, 2001), 3rd ed.
43. A. Mussot, E. Lantz, H. Maillotte, *et al.*, "Spectral broadening of a partially coherent cw laser beam in single-mode optical fibers," Opt. Express **12**(13), 2838–2843 (2004).
44. E. Treacy, "Optical pulse compression with diffraction gratings," IEEE J. Quantum Electron. **5**(9), 454–458 (1969).
45. E. Escoto, R. Jafari, G. Steinmeyer, *et al.*, "Linear chirp instability analysis for ultrafast pulse metrology," J. Opt. Soc. Am. B **37**(1), 74–81 (2020).